1. Introduction

Surface micro-topography has been shown to modulate cell adhesion and cell morphology (1), a phenomenon known as contact guidance (2-4). This effect is correlated with changes in gene (5) and protein expression (6). The use of micro-topography to modulate cell morphology, gene expression, protein expression, cell proliferation and cell differentiation has been applied to many studies aiming at tissue regeneration (7-9). Polycaprolactone (PCL) has been used widely in regenerative medicine because it is biocompatible and FDA approved. Furthermore, the imprinting of topographic features in the surface of PCL sheets is highly reproducible (10). Since PCL degrades with time post implantation (11), it presents an opportunity for gradual drug release (12).

In this study the integration of alternative medicine was applied to the grooved PCL sheets to observe the modulation of cell phenotype. The use of drug-impregnated composite biomaterials has been previously studied with various active agents, including bone morphogenic protein (13) and the antibiotics vancomycin (14) and tetracycline (15). In this study we focused on the use of a Chinese herb, Puerariae radix (the root of *Pueraria lobata* and *Pueraria mirifica* plants). This traditional Chinese medicine has been used for the treatment of various diseases and to promote bone healing for millenia and recent data suggest beneficial activity (16-20). The active ingredients have been identified as the isoflavones: puerarin, daidzin and daidzein, which have estrogenic activity (21-24). Puerariae radix has shown positive therapeutic effects in animal studies (25-27) and in cell culture studies, Puerariae radix was shown to induce osteogenic activity (20, 28-31). The studies showed that Puerariae radix had no effect on viability,

but enhanced Alkaline phosphatase (ALP activity), vascular endothelial growth factor (VEGF), bone matrix proteins such as osteocalcin (OCN), osteopontin (OPN), and collagen type I, and mineralization (20). A more detailed study using primary rat osteoblasts showed that puerarin caused a significant increase in cell viability, alkaline phosphatase (ALP) activity and mineral nodule formation by stimulating osteoblastic proliferation and activation of Akt in a phosphatidylinositol 3-kinase (PI3K)-dependent manner (30).

This report describes studies of Puerariae radix activity in composited polymers which could be applied in the field of tissue engineering. The puerariae powder was pressed into the melted PCL and the other side of the PCL was imprinted with micro-grooved features. This provided a bilayer material from which the active ingredients were expected to be gradually released from the PCL into the culture medium.

Differential In Gel Electrophoresis (DIGE) was exploited to compare the proteomic changes that are effected in response to surface topography and surface topography combined with Peurariae radix powder.

In this study, primary human STRO-1+ skeletal stem cells were used. The STRO-1+ population of human bone marrow is capable of osteogenic differentiation as well as reticular, chondrogenic and adipogenic differentiation (32, 33). These cells were separated from adult human bone marrow stromal cells (BMSCs) by the monoclonal

antibody (MAb) STRO-1, which recognizes a trypsin-resistant cell surface antigen present on a subpopulation of bone and marrow cells (34).

2. Materials and Methods

2.1 Material Fabrication

Quartz slides were cleaned in 7 parts Sulphuric acid and 1 part hydrogen peroxide for 5 mins. The slides were then spincoated with AZ primer at 4000 rpm for 30 secs. Shipley S1818 photoresist was next added, and the slides were spun for a further 30 secs. After spinning, the slides were soft baked at 90^{o}C for 30 mins. The samples were then exposed to uv light through a chrome mask (Hoya), patterned with 12.5μm wide line pattern. The exposed resist was developed using 1:1 (v/v) Shipley AZ developer: water. The slides were next etched to produce 2 μm deep grooves in a Plasma Technology RIE80 unit (Tri-chloromethane environment, pressure of 15 mTorr (1 Torr = 133.322 Pa), R.F. power of 100W, giving an etch rate of 25 nm/min). The mastering resist was then removed and the whole slide was etched for a further minute to produce a uniform chemistry. The fabricated slide has 12.5 μm width and 2 μm depth micro-grooved topography.

Cleaned polycaprolactone (PCL; Sigma-aldrich) sheet was melted then puerariae powder (purchased from Jishou City, Hunan province, China) was randomly spread onto the surface of the melted PCL at ratios 0, 1 and 2% w/w and then pressed with plain glass slide to impregnate puerariae powder into the melted PCL. The composite PCL sheet was cooled down then the glass slide was separated. For embossing, the PCL sheet was cut into 2 cm^2 squares before being cleaned with 75% ethanol following by deionized water

and blown to dry with cool air. The powder-free top side was embossed as describe in our previous study (6). Briefly, the PCL substrates were heated until they started to melt. Either the grooved or planar quartz slides were embossed onto the PCL substrates. PCL substrates were cooled down and the glass slides were removed.

2.2 Cell culture

Human bone marrow stromal cells were obtained from hematologically normal patients undergoing routine surgery. Only tissue that would have been discarded was used with the approval of the Southampton & South West Hants Local Research Ethics Committee. Primary cultures of bone marrow cells were established as previously described (35). The STRO-1+ fraction was isolated according to the method described by Howard et al (36).

STRO-1+ cells (2^{nd} passage) were cultured in 75 cm^2 tissue culture flasks. Culture was maintained in basal media (α-MEM containing 10% FBS and 2% antibiotics) at 37 ^{0}C, supplemented with 5% CO_2. Confluent cell sheets were trypsinized and $1x10^5$ cells were seeded onto 2 cm^2 PCL sheets with different features as following: 1) flat PCL, 2) micro-groove PCL, 3) micro-groove PCL with 1% puerariae powder and 4) micro-groove PCL with 2% puerariae powder. Materials were cultured in basal medium and maintained in culture with 5% CO_2 at 37 ^{o}C for 5 weeks. Medium was changed twice a week.

2.3 Toxicity and Cell Morphology

After 5 weeks, cell morphology and cell survival were observed by Coomassie staining. PCL sheets with cultured cells were fixed in 4% formaldehyde in PBS for 5 minutes. Cell staining was performed using 5% Coomassie blue in 40% methanol and 10% acetic acid for 5 minutes. The stained materials were washed twice in tap water. Pictures were taken by greyscale digital camera (Scion Corporation Model CFW-1310M).

2.4 Osteocalcin Staining

After 3 weeks of culture, the cells on the test materials were fixed in 4% formaldehyde in PBS, with 1% sucrose at 37°C for 15 min. When fixed, the samples were washed with PBS, and a permeabilizing buffer (10.3 g sucrose, 0.292 g NaCl, 0.06 g $MgCl_2$, 0.476 g Hepes buffer, 0.5 ml Triton X, in 100 ml water, pH 7.2) was added at 4 °C for 5 min. The samples were then incubated at 37 °C for 5 min in 1% BSA in PBS, followed by the addition of an anti-osteocalcin primary antibody (1:50 in 1% BSA in PBS, osteocalcin monoclonal anti-human raised in mouse (IgG), Autogen Bioclear, UK) for 1 h (37 °C). Simultaneously, rhodamine conjugated phalloidin was added for the duration of this incubation (1:100 in 1% BSA in PBS, Molecular Probes, Oregon, USA). The samples were next washed in 0.5% Tween 20 in PBS (5 min×3). A secondary, biotin conjugated antibody, (1:50 in 1% BSA in PBS, monoclonal horse anti-mouse (IgG), Vector Laboratories, Peterborough, UK) was added for 1 h (37 °C) followed by washing. A FITC conjugated streptavidin third layer was added (1:50 in 1% BSA in PBS, Vector Laboratories, Peterborough, UK) at 4 °C for 30 min, and a final wash was performed. Samples were then viewed by fluorescence microscope (Zeiss Axiovert 200 m).

2.5 Differential In Gel Electrophoresis

Two groups of experiment were set. First, the control group which protein extracts from flat PCL sheets were run against protein extracts from grooved PCL sheets. Second, the test group which protein extracts from flat PCL sheets were run against protein extracts from 2% w/w puerariae powder-impregnated PCL sheets as suggested in figure 1.

1) Protein Extraction: After 5 weeks culture, cell layer on PCL sheet were lysed in 1 ml of DIGE lysis buffer (7M Urea, 2M Thiourea, 4% CHAPS and 30 mM Tris-base pH 8.0) with 1X final concentration of general purposes protease inhibitor cocktail (Sigma-Aldrich). The cell suspension was left at room temperature for 1 hour with vigorous mixing every 20 minutes. The PCL sheets were taken out and the suspension was then centrifuged at 2,100 rpm for 10 minutes to remove insoluble material. Proteins were then precipitated from the supernatant by addition of 4 volumes of 100% cold acetone. After centrifugation, the protein pellets were washed in 80% acetone and re-suspended in DIGE lysis buffer. The Bradford protein assay was used to determine the amount of protein extracted from each material. Briefly, varying concentrations of BSA (50, 25, 12.5, 6.25 and 3.125 μg/ml) were prepared and used as a standard curve. 10 μl of each standard and sample was mixed with 200 μl of protein assay reagent (Bio-Rad). The reaction was left to progress at room temperature for 5 minutes. Absorbance was measured at 595 nm. Protein concentrations of the protein extracts from the test materials were determined from the standard curve.

2) Saturation labelling: 5 μg of the extracted proteins were added into sterile microfuge tubes. Protein in each tube was reduced with 1 μl of 2 mM TCEP. The reactions were incubated at 37^0C in the dark for 1 hour. Protein in each tube was labeled with the required volumes (2 μl) of Cy3 and Cy5 in the dark for 30 minutes (Typically, 5 μg of protein requires 2 nmol TCEP and 4 nmol of CyDye). Equal volumes of 2X sample buffer (7M Urea, 2M Thiourea, 4% w/v CHAPS, 2% w/v IPG buffer pH 4-7 and 2% w/v DTT) were added to stop the reactions. Proteins labeled with Cy3 and Cy5 were mixed together. 2D-Gel electrophoresis was performed.

3) 2D-Gel Electrophoresis: First dimension isoelectric focusing (IEF) was performed on IPG strips (24 cm; linear gradient pH 4–7) using an Ettan IPGphor system (GE-Healthcare). IEF was performed using the following voltage program: 30 V constant for 12 h, 300 V constant for 1 h, linear up to 600 V over 1 h, linear up to 1,000 V over 1 h, linear up to 8,000 V over 3 h, then 8,000 V constant for 8.30 h. The current was limited to 50 μA *per* strip and the temperature maintained at 20 ^{0}C. After focusing, strips were equilibrated for 15 min in 5 ml of reducing solution (6 M urea, 100 mM Tris-HCl pH 8, 30% v/v glycerol, 2% w/v SDS, 5 mg/mL DTT). For second dimension SDS-PAGE, IPG strips were placed on the top of 12% acrylamide gels cast in low fluorescence glass plates and then sealed by 0.5% (w/v) agarose overlay solution. Gels were run at constant power 50 W/gel until the bromophenol blue tracking front had reached the base of the gel. Fluorescence images of the gels were obtained by scanning on a Typhoon 9400 scanner (GE Healthcare). Cy3 and Cy5 images were scanned at 532 nm/580 nm and 633 nm/670 nm excitation/emission wavelengths respectively, at a 100 mm resolution. Image analysis

and statistical quantification of relative protein expression was performed using DeCyder^{TM} 7 software (GE Healthcare).

4) Preparative 2D gel: 500 μg protein extracted from human STRO-1+ cultured in a tissue culture flask was reduced by 10 μl of 20 mM TCEP and then labeled with 10 μl of 20 mM Cy3 DIGE flour. After this, 2D-Gel Electrophoresis was performed and the gel scanned as described above. The preparative gel image was matched with analytical DIGE gel images and the spots of interest were selected for further analysis. A pick list was generated, containing gel co-ordinates that were used to direct spot cutting for spots of interest. Gel spots were excised using an Ettan Spot Handling Workstation (Amersham Biosciences, UK) and each gel piece was placed in a separate well of a 96-well plate. Gel pieces were washed three times in 100 μl of 50 mM ammonium bicarbonate, 50% v/v methanol and then twice in 100 μl 75% v/v acetonitrile, before drying. Gel pieces were rehydrated with trypsin solution (20 μg trypsin/ml 20 mM ammonium bicarbonate), and incubated for 4 h at 37 ^{o}C. Peptides were extracted from the gel pieces by washing twice in 100 μl of 50% v/v acetonitrile / 0.1% v/v trifluoroacetic acid, before being transferred in solution to a fresh 96 well plate and dried before mass spectrometric (MS) analysis.

5) MS/MS and Database Analysis. Tryptic peptide solutions were mixed at a 1:1 ratio with 5 mg/mL α–cyano-4-hydroxycinnamic acid (CHCA) matrix in 0.3% TFA, and spotted on stainless steel MALDI sample plates (Applied Biosystems, Framingham, MA). Peptide mixtures were then analyzed using MALDI/TOF/TOF (4700 Proteomics Analyzer, Applied Biosystems, Framingham, MA). MALDI-TOF spectra were collected from m/z 800 – 4000 and up to 10 peaks were selected for MS/MS analysis. Protein

identification was performed using Global Proteome Server Explorer software (Applied Biosystems, Framingham, MA) utilizing the NCBI Reference Sequence human protein database. The identification was assigned to a protein spot feature if the protein score was calculated to be greater than 50, correlating to a confidence interval of 95%. Protein identifications were assigned using the Mascot search engine, which gives each protein a probability based MOWSE score. In all cases variable methionine oxidation was used for searches. Only proteins identified with a significant score ($p = <0.05$) were included, corresponding to a MOWSE score greater than 66.

2.6 HPLC detection of isoflavone in growth media

For standard, 130 mg of puerariae powder was dissolved in 2 ml of distilled water and mixed vigorously for 30 minutes before 6 ml of methanol was added. The solution was left at room temperature for 1 hour with vigorously mixing every 20 minutes. Powder solution was spun down at 2100 rpm for 20 min. Supernatant was collected and aliquoted into eppendorf tubes for 1 ml/vial. All vials were dried by speed vacuum centrifugation. For culture medium, PCL sheets (with or without powder) were incubated with 2 ml medium at 37 ^{o}C for 2 weeks. 2 ml of medium was collected and 6 ml of methanol was added and processed with the same procedure for standard.

200 μl methanol was added to a dried standard vial and 50 μl methanol was added to a dried sample vial, due to the anticipated reduction in concentration of the active ingredient, 10 μl of each sample was used to perform the reversed phase separation.

Reversed phase HPLC was performed as described in Jiang et al (37). Briefly, buffers consisted of 0.2% acetic acid (A) and acetonitrile (B). The gradient consisted of a 10 minute isocratic at 15% B, followed by a linear gradient from 15% to 30% B in 2.5 minutes, an isocratic at 30% B for 10 minutes, a linear gradient from 30% B to 15% B in 2.5 minutes, and finally an isocratic at 15% B for 5 minutes. The HPLC system used was an UltiMate (Dionex) running at 200 μl/min with a 4.6mm x 25cm C18 reversed phase column (Phenomenex). Detection was performed using an UltiMate UV absorbance detector at a wavelength of 254 nm.

2.7 The Mass Identification of isoflavones in crude extract

The preparation of DHB and sample was modified from (38): the matrix solution contained 10−15 mg/mL DHB in 10% ethanol. The ratio of matrix solution to clude extracts was 1:1. The mixture (1.5 μL) was applied to a MALDI-TOF MS plate and air-dried.

3. Results

3.1 Atomic Force Microscopy

The AFM images (figure 2) showed that the grooved topography from quartz slide was successfully embossed onto the PCL sheet. Furthermore, the images indicate that herbal particles at the bottom side of PCL sheets did not affect the surface topography. The surface roughness of the control PCL sheet was evaluated and the typical Ra was 28.406.

3.2 Cell morphology and Toxicity

Coomassie blue staining after 5 weeks indicated that human STRO-1+ cells on the flat control were observed to be well spread whilst STRO-1+ cells on all micro-grooved PCL were contact guided along the grooved direction (figure 3). Confluent cell layers (90%+) were observed on control, grooved PCL, 1% w/w puerariae powder-impregnated grooved PCL and 2% w/w puerariae powder-impregnated grooved PCL. This result indicates that the puerariae powder at concentrations of 1 and 2% w/w did not affect cell growth and cell viability. Thus, only 2% w/w puerariae powder-impregnated grooved PCL was chosen to use in the subsequent experiments.

3.3 Osteocalcin staining

Osteocalcin staining was performed after 3 weeks culture on control flat PCL sheet, grooved PCL and 2% w/w puerariae powder-impregnated grooved PCL (figure 4). Osteocalcin expression was not observed on control PCL whilst weak expression was observed on grooved PCL. Positive osteocalcin was clearly observed in cells cultured on 2% w/w grooved puerariae powder-impregnated sheets (figure 4C).

3.4 Differential In Gel Electrophoresis (DIGE)

DIGE results showed that the expression of a number of proteins (figure 5) was significantly modulated following the culture of human STRO-1+ cells on micro-grooved PCL (with/without puerariae powder), in comparison to STRO-1+ cells cultured on flat control as a standard. A list of proteins that showed modulated expression upon exposure to 2% w/w puerariae powder-impregnated grooved PCL compared against grooved PCL are presented in table 1.

Protein descriptions

1. Gelsolin: Gelsolin was down-regulated in all three gels of the test group when compared to the control group. Gelsolin is an actin-binding protein that nucleates actin polymerization and severs and caps actin filaments in a calcium dependent manner (39). Under depolymerizing conditions, these gelsolin-capped ends allow the disassembly of populations of actin filaments by subunit loss from the pointed ends. Under polymerizing conditions, gelsolin exhibits calcium-dependent actin nucleating activity and stimulates actin filament formation from monomers (40).

2. Tubulin: Tubulin was down-regulated in the test group when compared to the control group. Previous studies have demonstrated a correlation between the state of organization and the expression of the respective cytoskeletal protein by showing that depolymerization of microtubules leads to a rapid decrease in new tubulin synthesis (41).

Non-polymerized tubulin represses its own synthesis (42). Microtubule depolymerization induces mitotic arrest and suppresses tumor cell growth (43).

3. Vinculin: Vinculin was up-regulated only in the test group when compared to the control group. Vinculin is a major component of adhesion plaques and cell-cell junctions. The existence of a coordinated mechanism(s) of actin polymerization-dependent regulation of actin and vinculin synthesis was suggested by previous study (44). A stabilizer of polymerized actin that increased the level of assembled actin, resulted in elevated vinculin synthesis (44).

4. Vimentin: Vimentin was up-regulated on grooved-materials and 2% puerariae powder impregnated-grooved PCL. The expression of vimentin in the test group was approximately 12-times higher compared to the control group. Vimentin and intermediate filaments were also used as a differentiation marker in a number of cell types. The differentiation process of optic vesicle epithelium into neural retina is influenced by the amount of vimentin in epithelial cells (45). In the clonal osteoblast-like cell line MC3T3-E1, cDNAs of vimentin were up-regulated in differentiation compared with proliferation (46). Vimentin expression could thus play a role at an advanced stage of skeletal stem cell differentiation (47).

5. Actin: Actin and profilin-beta-actin were up-regulated in all three gels of the test group in comparison to the control group. Previous studies suggested that increased actin polymerization resulted in smooth muscle cell differentiation and increased actin expression (48). Actin assembly is regulated by controlling the balance between polymerized and non-polymerized actin and stabilization of polymerized actin results in a significant increase in actin synthesis (44).

6. Laminin binding protein (Laminin receptor): Laminin receptor was up-regulated in the test group when compared to the control group. Estrogen decreases laminin expression (49). However, Laminin-111 suppress the expression of estrogen receptor (ERbeta1) at the mRNA level (50). Laminin binding to its receptors acts via phosphatidylinositol-3-kinase/Akt (PI3K/Akt)(51, 52), as does estrogen and phytoestrogen (30, 53, 54). The augmentation of laminin receptor mRNA by estrogen and progesterone treatment in hormone receptor-positive human breast cancer cell lines has been reported (55).

7. Annexin V (AnxV): Annexin V was up-regulated in two gels of the test group when compared to the control group. AnxV is a calcium-dependent phospholipid binding protein which functions as a Ca2+ selective ion channel. Annexin V has the ability to interact with both extracellular matrix proteins and cytoskeletal elements. Overexpression of annexin V also resulted in up-regulation of osteocalcin (56).

8. Cofilin: Cofilin was up-regulated only in the test group. Cofilin expression and phospho-cofilin were strongly increased cell culture conditions favoring myofibroblast differentiation (57). Cofilin is phosphorylated at serine 3 by LIM domain kinase (LIMK) and Testis-specific kinase (TESK) and that inhibits cofilin binding to F-actin, leading to F-actin stabilization. Cofilin dephosphorylation by slingshot (SSH) and chronophin (CIN) stimulates F-actin depolymerization and severing (58).

9. Myosin head domain containing protein: Myosin head functions through its ATPase reaction as a force generator and as a mechanosensor, and two myosin heads work together in moving along an actin filament which is involved in a wide range of transport and contractile activities in cells (59, 60).

3.5 HPLC detection of isoflavone in growth media

Herein, the reported peaks were, in general, broader than those described in previous studies (37), probably as a consequence of the decreased flow-rate used. However, a strong doublet corresponding to an isoflavone/unknown pair is seen at the same retention time, and possessing equivalent peak area to that described in the Jiang paper (37). Figure 6 shows typical chromatograms consisting of a) the puerariae standard, b) serum-free growth medium control, c) serum-free growth medium from puerariae-impregnated grooved-PCL, d) serum-containing growth medium control e) serum-containing growth medium from puerariae-impregnated grooved-PCL.

The isoflavone doublet can clearly be observed as a pair of slightly broad, low intensity peaks corresponding exactly in retention time and relative abundance to the standard in the serum-free growth medium from puerariae-impregnated grooved-PCL, where as it is unobserved in both control samples. The isoflavone peak does not appear in the serum-containing growth medium from impregnated grooved-PCL, but this is likely to be a consequence of the reduced abundance (50%) of the compound in comparison to serum-free medium sample.

3.6 Mass spectrometry of the crude extract

The mass spectrum of the crude extract showed 3 major peaks of 413.2102, 417.0634 and 429.1615 (figure 8). Data from Massbank records indicates that the negative ionization

mass spectrum of puerarin is 415.1004 $(M-H)^-$ whilst the positive ionization mass spectrum is 417.1180 $(M+H)^+$ and the exact mass is 416.11073 (by LC-ESI-IT-TOF-MS). This study found a peak at 417.0634 (by MALDI-TOF), which is closed to the positive ionization mass spectrum (417.1180) from the Massbank record.

Discussion

Coomassie staining indicated that cell growth and cell survival on flat PCL, grooved-PCL, 1% puerariae powder impregnated-grooved-PCL and 2% puerariae powder impregnated-grooved-PCL were similar. Hence the 2% puerariae powder impregnated-grooved-PCL was chosen to compare against grooved-PCL using flat surfaces as a standard to study the integrated effect between isoflavones and topographical contact guidance. The study was separated into two groups (figure 1). Along with the test group (in which 2% puerariae powder impregnated-grooved-PCL was run against flat PCL), the control group (in which normal grooved PCL was run against flat PCL) was used to provide the fundamental effect of cell contact guidance on the skeletal stem cells.

Puerariae radix (PR) is a popular natural herb and a traditional food in China. Isoflavones are a subclass of flavonoids. Isoflavones such as puerarin, daidzin, and daidzein are commonly regarded as phytoestrogens found in PR owing to their estrogenic activity in certain animal models (61, 62). Results from cell cycle distribution indicated that isoflavones from puerariae radix mediated cell cycle arrest in the G2/M phase (63). The study of estrogen (17β-Estradiol) treatment on osteoblastic MBA-15 cells derived from marrow stromal origin resulted in reduction in expression of tubulin (64) as found in this

study (7-fold). These previous studies suggested the report of tubulin down-regulation in this study, as cell cycle arrest in the G2/M can result in the depolymerization of microtubules to tubulin monomer which suppresses its own synthesis, can result in cell differentiation.

Up-regulation of vimentin was even stronger on impregnated-grooved-PCL (12 fold compared to control) (table 1) which might indicated an advanced stage of differentiation (47). These results may indicate that the impregnated-grooved-PCL caused cell cycle arrested and induced differentiation.

Down-regulation of gelsolin and up-regulation actin together with annexin V were seen on 2% puerariae powder impregnated-grooved-PCL when compared to grooved PCL. These results indicated dynamic polymerizing condition of actin which happened in differentiation state (65) and because gelsolin works in a calcium-dependent manner (39) thus this event supported the up-regulation of annexin V. Furthermore, up-regulation of annexin V was related with the up-regulation of osteocalcin in the cultured cells (56) which was supported by osteocalcin staining. However, changes in expressions of these proteins were not significant. It was likely that dynamic polymerizing condition of actin and differentiation of the cultured cells were also observed on normal grooved-PCL (6, 66) which could be observed by the modest osteocalcin staining (figure 4B).

At 3 weeks, osteocalcin staining for bone extracellular matrix indicated that 2% puerariae powder impregnated-grooved-PCL inserted stronger effect for osteocalcin production

when compared to normal micro-grooved PCL and flat PCL which indicated that the impregnated-grooved-PCL modulated phenotypic change in the cultured cells.

We postulate that whilst the microgrooves clearly had effects on the proteome and contact guidance of STRO-1+ cells, it is possible that more fibroblastic differentiation was induced. Fibroblasts adopt a biopolarised, contact guided morphology *in vivo*. The cells on the grooves are reminiscent of such a natural morphology. This is somewhat contrast with initial consideration in our previous study where unselected osteoprogenitor cells of the bone marrow were shown to form mineral nodules on microgrooves (6). However, it must be noted that unselected human bone marrow is a heterogeneous population that contains cells already committed to the osteoblast lineage, and indeed, mature osteobalsts. The STRO-1+ selected skeletal stem cells, however, enriched of osteoprogenetors and represent an earlier bone cell population. Puerariae powder and micro-grooved topography clearly modulated the skeletal cell proteome which indicated that on the surfaces cells were differentiating. However, from the protein expression profile and the histologic analysis, it was unclear which cells predominated on the surfaces. Since human STRO-1+ population are capable of osteogenic differentiation as well as reticular, chondrogenic and adipogenic differentiation. Additionally, the herb itself has a broad-effect on cell differentiation i.e. neurogenic has been suggested by others (67) and osteogenic differentiation (20). Furthermore, previous studies have also indicated that activation of a focal adhesion kinase (FAK) and extracellular signal-related kinase (ERK) dependent pathway by laminin binding to LG3 integrin binding domain mediated osteogenic differentiation but did not increase matrix mineralization,

demonstrating that the activation of FAK and ERK signaling is not sufficient to induce complete osteogenic differentiation in vitro (68). A previous study indicated that phytoestrogen, puerarin, act via phosphatidylinositol-3-kinase/Akt (PI3K/Akt) (54) thus complete osteogenic differentiation might need more than one signaling pathway working in concert with each other. In this study even the osteocalcin staining was positive at 3 weeks but the study of the effect of puerariae radix on bone tissue engineering might need partial committed like unselected osteoprogenitor cells.

The combination of micro-grooved substrate topography and puerariae powder appears to exert a significant effect on skeletal stem cells beyond the topographical cues stimulating the skeletal stem cells to change their proteomic regulation. Nevertheless, there is a need to study the effects of puerariae powder and topographical cues using unselected osteoprogenitors to provide heterogeneous populations. Such studies allow examination of the *in vivo* scenario and can be informative in delineating cell selection/differentiation strategies.

Conclusions

Topographical cues together with impregnated-puerariae powder induced changes in the skeletal stem cell proteome. The use of liquid chromatography and mass spectrometry indicated that the active ingredients in puerariae powder were released into the culture medium. This study suggests an alternative approach using puerariae powder in materials research and the potential therein for such approaches to modulate cell phenotype and function.

Legends

Figure 1. Working diagram: This diagram presented that DIGE experiment was separated into control group and test group. The control group provided the fundamental effect of micro-groove topography whilst the test group provided the integration effect of micro-groove topography and puerariae powder.

Figure 2. The Atomic Force Microscope analysis: (A) control flat PCL sheet, (B) grooved PCL, (C) 1% w/w puerariae powder-impregnated grooved PCL and (D) 2% w/w puerariae powder-impregnated grooved PCL.

Figure 3. Cell morphology: (A) control flat PCL sheet, (B) grooved PCL, (C) 1% w/w puerariae powder-impregnated grooved PCL and (D) 2% w/w puerariae powder-impregnated grooved PCL. Confluent cell layers (90%+) were observed on all materials. Puerariae powder at concentrations of 1 (C) and 2% (D) w/w did not affect cell growth and cell survival.

Figure 4. Osteocalcin staining: (A) control flat PCL sheet, (B) grooved PCL, (C) 2% w/w puerariae powder-impregnated grooved PCL. No positive osteocalcin staining was observed on flat PCL whilst slight positive result (small green spots) was found on grooved PCL. Strong positive osteocalcin was clearly observed on 2% w/w puerariae powder-impregnated grooved PCL (green spots).

Figure 5. DIGE analysis: Protein spots with changed expression were presented on DIGE preparative gel image. The numbers represented proteins with changes in their expression i.e. 1. gelsolin, 2. tubulin, 3. vinculin, 4. vimentin, 5. actin, 6. Laminin-binding protein, 7 annexin V, 8. cofilin and 9. myosin head domain containing protein.

Figure 6. HPLC detection of isoflavones at 254nm: Black lines denote UV absorbance chromatograms. Samples consist of a) puerariae standard, b) serum-free medium control, c) serum-free medium with puerariae powder-impregnated micro-grooved PCL d) serum-containing medium control, e) serum-containing medium with puerariae powder-impregnated micro-grooved PCL. Isoflavones is the first peak in the doublet (circled with red in (a)), and is clearly visible, but low abundance (circled in blue) in (c).

Figure 7. Mass Spectrum of isoflavones in clued extract: Isoflavones peak at 417.0634 m/z was detected by MALDI-TOF-TOF.

Table 1. Protein expression profiles: protein expression profiles of cells cultured on 2% puerariae powder impregnated-grooved PCL were compared against grooved PCL sheets using protein extract from flat PCL as a standard. Three replicates of DIGE analysis were performed. Average volume (AV) ratios of protein expression together with p-values were presented. Note that p-values > 0.05 were marked with *.

Reference

1. Meredith DO, Eschbach L, Riehle MO, Curtis AS, Richards RG. Microtopography of metal surfaces influence fibroblast growth by modifying cell shape, cytoskeleton, and adhesion. J Orthop Res. 2007 Nov;25(11):1523-33.
2. Curtis AS, Wilkinson CD. Reactions of cells to topography. J Biomater Sci Polym Ed. 1998;9(12):1313-29.
3. Clark P, Connolly P, Curtis AS, Dow JA, Wilkinson CD. Topographical control of cell behaviour. I. Simple step cues. Development. 1987 Mar;99(3):439-48.
4. Clark P, Connolly P, Curtis AS, Dow JA, Wilkinson CD. Topographical control of cell behaviour: II. Multiple grooved substrata. Development. 1990 Apr;108(4):635-44.
5. Dalby MJ, Riehle MO, Yarwood SJ, Wilkinson CD, Curtis AS. Nucleus alignment and cell signaling in fibroblasts: response to a micro-grooved topography. Exp Cell Res. 2003 Apr 1;284(2):274-82.
6. Kantawong F, Burchmore R, Wilkinson CD, Oreffo RO, Dalby MJ. Differential in-gel electrophoresis (DIGE) analysis of human bone marrow osteoprogenitor cell contact guidance. Acta Biomater. 2009 May;5(4):1137-46.
7. Anselme K, Bigerelle M, Noel B, Iost A, Hardouin P. Effect of grooved titanium substratum on human osteoblastic cell growth. J Biomed Mater Res. 2002 Jun 15;60(4):529-40.
8. Zhu X, Chen J, Scheideler L, Altebaeumer T, Geis-Gerstorfer J, Kern D. Cellular reactions of osteoblasts to micron- and submicron-scale porous structures of titanium surfaces. Cells Tissues Organs. 2004;178(1):13-22.
9. Zhu X, Chen J, Scheideler L, Reichl R, Geis-Gerstorfer J. Effects of topography and composition of titanium surface oxides on osteoblast responses. Biomaterials. 2004 Aug;25(18):4087-103.
10. Gadegaard N. Atomic force microscopy in biology: technology and techniques. Biotech Histochem. 2006 Mar-Jun;81(2-3):87-97.
11. Lam CX, Hutmacher DW, Schantz JT, Woodruff MA, Teoh SH. Evaluation of polycaprolactone scaffold degradation for 6 months in vitro and in vivo. J Biomed Mater Res A. 2008 Jul 21.
12. Zalfen AM, Nizet D, Jerome C, Jerome R, Frankenne F, Foidart JM, et al. Controlled release of drugs from multi-component biomaterials. Acta Biomater. 2008 Nov;4(6):1788-96.
13. Li J, Bai L, Cui S, Wang H, Xu X. [Comparison between gene therapy and gradual release carrier for bone morphogenetic protein-2 in repairing bone defects]. Sheng Wu Yi Xue Gong Cheng Xue Za Zhi. 2007 Jun;24(3):667-70.
14. Kim HW, Lee EJ, Jun IK, Kim HE, Knowles JC. Degradation and drug release of phosphate glass/polycaprolactone biological composites for hard-tissue regeneration. J Biomed Mater Res B Appl Biomater. 2005 Oct;75(1):34-41.
15. Kim HW, Knowles JC, Kim HE. Hydroxyapatite/poly(epsilon-caprolactone) composite coatings on hydroxyapatite porous bone scaffold for drug delivery. Biomaterials. 2004 Mar-Apr;25(7-8):1279-87.
16. Manonai J, Seif C, Bohler G, Junemann KP. The effect of Pueraria mirifica on cytologic and urodynamic findings in ovariectomized rats. Menopause. 2008 Dec 17.

17. Okamura S, Sawada Y, Satoh T, Sakamoto H, Saito Y, Sumino H, et al. Pueraria mirifica phytoestrogens improve dyslipidemia in postmenopausal women probably by activating estrogen receptor subtypes. Tohoku J Exp Med. 2008 Dec;216(4):341-51.
18. Zhang HY, Liu YH, Wang HQ, Xu JH, Hu HT. Puerarin protects PC12 cells against beta-amyloid-induced cell injury. Cell Biol Int. 2008 Oct;32(10):1230-7.
19. Zhang SY, Chen G, Wei PF, Huang XS, Dai Y, Shen YJ, et al. The effect of puerarin on serum nitric oxide concentration and myocardial eNOS expression in rats with myocardial infarction. J Asian Nat Prod Res. 2008 Mar-Apr;10(3-4):373-81.
20. Huh JE, Yang HR, Park DS, Choi DY, Baek YH, Cho EM, et al. Puerariae radix promotes differentiation and mineralization in human osteoblast-like SaOS-2 cells. J Ethnopharmacol. 2006 Apr 6;104(3):345-50.
21. Cherdshewasart W, Sriwatcharakul S, Malaivijitnond S. Variance of estrogenic activity of the phytoestrogen-rich plant. Maturitas. 2008 Dec 20;61(4):350-7.
22. Fang C, Wan X, Tan H, Jiang C. Separation and determination of isoflavonoids in several kudzu samples by high-performance capillary electrophoresis (HPCE). Ann Chim. 2006 Jan-Feb;96(1-2):117-24.
23. Prasain JK, Reppert A, Jones K, Moore DR, 2nd, Barnes S, Lila MA. Identification of isoflavone glycosides in Pueraria lobata cultures by tandem mass spectrometry. Phytochem Anal. 2007 Jan;18(1):50-9.
24. Rong H, Stevens JF, Deinzer ML, Cooman LD, Keukeleire DD. Identification of isoflavones in the roots of Pueraria lobata. Planta Med. 1998 Oct;64(7):620-7.
25. Heng LS, Lan BS, Jia Z, Wang PF, Fan LY. [Protective effect of puerarin on the secondary spinal cord injury in rats]. Zhong Yao Cai. 2009 Mar;32(3):395-7.
26. Pan ZY, Bao ZS, Wu ZM, Wang XM, Zheng JZ, Shen YL, et al. The myocardial protective effects of puerarin on STZ-induced diabetic rats. Fen Zi Xi Bao Sheng Wu Xue Bao. 2009 Apr;42(2):137-44.
27. Gao L, Ji X, Song J, Liu P, Yan F, Gong W, et al. Puerarin protects against ischemic brain injury in a rat model of transient focal ischemia. Neurol Res. 2009 May;31(4):402-6.
28. Li B, Yu S. [Effect of puerarin on the bone metabolism in vitro]. Beijing Da Xue Xue Bao. 2003 Feb 18;35(1):74-7.
29. Wong R, Rabie B. Effect of puerarin on bone formation. Osteoarthritis Cartilage. 2007 Aug;15(8):894-9.
30. Zhang Y, Zeng X, Zhang L, Zheng X. Stimulatory effect of puerarin on bone formation through activation of PI3K/Akt pathway in rat calvaria osteoblasts. Planta Med. 2007 Apr;73(4):341-7.
31. Zang HM, Chen JC, Liu YH, Wang KZ. [Experimental study of the effects of puerarin on biological characters of osteoblasts in vitro]. Zhongguo Zhong Yao Za Zhi. 2005 Dec;30(24):1947-9.
32. Gronthos S, Graves SE, Ohta S, Simmons PJ. The STRO-1+ fraction of adult human bone marrow contains the osteogenic precursors. Blood. 1994 Dec 15;84(12):4164-73.

33. MacArthur BD, Tare RS, Murawski K, Oreffo RO. Identification of candidate regulators of multipotency in human skeletal progenitor cells. Biochem Biophys Res Commun. 2008 Dec 5;377(1):68-72.
34. Stewart K, Walsh S, Screen J, Jefferiss CM, Chainey J, Jordan GR, et al. Further characterization of cells expressing STRO-1 in cultures of adult human bone marrow stromal cells. J Bone Miner Res. 1999 Aug;14(8):1345-56.
35. Yang XB, Roach HI, Clarke NM, Howdle SM, Quirk R, Shakesheff KM, et al. Human osteoprogenitor growth and differentiation on synthetic biodegradable structures after surface modification. Bone. 2001 Dec;29(6):523-31.
36. Howard D, Partridge K, Yang X, Clarke NM, Okubo Y, Bessho K, et al. Immunoselection and adenoviral genetic modulation of human osteoprogenitors: in vivo bone formation on PLA scaffold. Biochem Biophys Res Commun. 2002 Nov 29;299(2):208-15.
37. Jiang RW, Lau KM, Lam HM, Yam WS, Leung LK, Choi KL, et al. A comparative study on aqueous root extracts of Pueraria thomsonii and Pueraria lobata by antioxidant assay and HPLC fingerprint analysis. J Ethnopharmacol. 2005 Jan 4;96(1-2):133-8.
38. Wang J, Sporns P. MALDI-TOF MS analysis of isoflavones in soy products. J Agric Food Chem. 2000 Dec;48(12):5887-92.
39. Khaitlina S, Walloscheck M, Hinssen H. Calcium-induced conformational changes in the C-terminal half of gelsolin stabilize its interaction with the actin monomer. Biochemistry. 2004 Oct 12;43(40):12838-45.
40. McGough AM, Staiger CJ, Min JK, Simonetti KD. The gelsolin family of actin regulatory proteins: modular structures, versatile functions. FEBS Lett. 2003 Sep 25;552(2-3):75-81.
41. Ben-Ze'ev A. Application of two-dimensional gel electrophoresis in the study of cytoskeletal protein regulation during growth activation and differentiation. Electrophoresis. 1990 Mar;11(3):191-200.
42. Cleveland DW, Lopata MA, Sherline P, Kirschner MW. Unpolymerized tubulin modulates the level of tubulin mRNAs. Cell. 1981 Aug;25(2):537-46.
43. Shi YQ, Zhu CJ, Yuan HQ, Li BQ, Gao J, Qu XJ, et al. Marchantin C, a novel microtubule inhibitor from liverwort with anti-tumor activity both in vivo and in vitro. Cancer Lett. 2008 Dec 16.
44. Bershadsky AD, Gluck U, Denisenko ON, Sklyarova TV, Spector I, Ben-Ze'ev A. The state of actin assembly regulates actin and vinculin expression by a feedback loop. J Cell Sci. 1995 Mar;108 (Pt 3):1183-93.
45. Iwatsuki H, Sasaki K, Suda M, Itano C. Vimentin intermediate filament protein as differentiation marker of optic vesicle epithelium in the chick embryo. Acta Histochem. 1999 Nov;101(4):369-82.
46. Kitching R, Qi S, Li V, Raouf A, Vary CP, Seth A. Coordinate gene expression patterns during osteoblast maturation and retinoic acid treatment of MC3T3-E1 cells. J Bone Miner Metab. 2002;20(5):269-80.
47. Rius C, Aller P. Vimentin expression as a late event in the in vitro differentiation of human promonocytic cells. J Cell Sci. 1992 Feb;101 (Pt 2):395-401.

48. Mack CP, Somlyo AV, Hautmann M, Somlyo AP, Owens GK. Smooth muscle differentiation marker gene expression is regulated by RhoA-mediated actin polymerization. J Biol Chem. 2001 Jan 5;276(1):341-7.
49. Dixon A, Maric C. 17beta-Estradiol attenuates diabetic kidney disease by regulating extracellular matrix and transforming growth factor-beta protein expression and signaling. Am J Physiol Renal Physiol. 2007 Nov;293(5):F1678-90.
50. Neubauer H, Ruoff A, Paessler N, Solomayer E, Wallwiener D, Fehm T. A laminin-rich basement membrane matrix influences estrogen receptor beta expression and morphology of MDA-MB-231 breast cancer cells. Oncol Rep. 2009 Feb;21(2):475-81.
51. Wang YG, Ji X, Pabbidi M, Samarel AM, Lipsius SL. Laminin acts via focal adhesion kinase/phosphatidylinositol-3' kinase/protein kinase B to down-regulate beta1-adrenergic receptor signalling in cat atrial myocytes. J Physiol. 2009 Feb 1;587(Pt 3):541-50.
52. Xiong Y, Zhou Y, Jarrett HW. Dystrophin glycoprotein complex-associated Gbetagamma subunits activate phosphatidylinositol-3-kinase/Akt signaling in skeletal muscle in a laminin-dependent manner. J Cell Physiol. 2009 May;219(2):402-14.
53. Hua K, Feng W, Cao Q, Zhou X, Lu X, Feng Y. Estrogen and progestin regulate metastasis through the PI3K/AKT pathway in human ovarian cancer. Int J Oncol. 2008 Nov;33(5):959-67.
54. Hwang YP, Jeong HG. Mechanism of phytoestrogen puerarin-mediated cytoprotection following oxidative injury: estrogen receptor-dependent up-regulation of PI3K/Akt and HO-1. Toxicol Appl Pharmacol. 2008 Dec 15;233(3):371-81.
55. Castronovo V, Taraboletti G, Liotta LA, Sobel ME. Modulation of laminin receptor expression by estrogen and progestins in human breast cancer cell lines. J Natl Cancer Inst. 1989 May 10;81(10):781-8.
56. Wang W, Xu J, Kirsch T. Annexin V and terminal differentiation of growth plate chondrocytes. Exp Cell Res. 2005 Apr 15;305(1):156-65.
57. Pho M, Lee W, Watt DR, Laschinger C, Simmons CA, McCulloch CA. Cofilin is a marker of myofibroblast differentiation in cells from porcine aortic cardiac valves. Am J Physiol Heart Circ Physiol. 2008 Apr;294(4):H1767-78.
58. Huang TY, DerMardirossian C, Bokoch GM. Cofilin phosphatases and regulation of actin dynamics. Curr Opin Cell Biol. 2006 Feb;18(1):26-31.
59. Skau KI, Hoyle RB, Turner MS. A kinetic model describing the processivity of myosin-V. Biophys J. 2006 Oct 1;91(7):2475-89.
60. Jackson del R, Jr., Baker JE. The energetics of allosteric regulation of ADP release from myosin heads. Phys Chem Chem Phys. 2009 Jun 28;11(24):4808-14.
61. Wang X, Wu J, Chiba H, Umegaki K, Yamada K, Ishimi Y. Puerariae radix prevents bone loss in ovariectomized mice. J Bone Miner Metab. 2003;21(5):268-75.
62. Wang X, Wu J, Chiba H, Yamada K, Ishimi Y. Puerariae radix prevents bone loss in castrated male mice. Metabolism. 2005 Nov;54(11):1536-41.

63. Lin YJ, Hou YC, Lin CH, Hsu YA, Sheu JJ, Lai CH, et al. Puerariae radix isoflavones and their metabolites inhibit growth and induce apoptosis in breast cancer cells. Biochem Biophys Res Commun. 2009 Jan 23;378(4):683-8.
64. Benayahu D. Estrogen effects on protein expressed by marrow stromal osteoblasts. Biochem Biophys Res Commun. 1997 Apr 7;233(1):30-5.
65. Higuchi C, Nakamura N, Yoshikawa H, Itoh K. Transient dynamic actin cytoskeletal change stimulates the osteoblastic differentiation. J Bone Miner Metab. 2009;27(2):158-67.
66. Hamilton DW, Riehle MO, Monaghan W, Curtis AS. Articular chondrocyte passage number: influence on adhesion, migration, cytoskeletal organisation and phenotype in response to nano- and micro-metric topography. Cell Biol Int. 2005 Jun;29(6):408-21.
67. Chen HT, Yao CH, Chao PD, Hou YC, Chiang HM, Hsieh CC, et al. Effect of serum metabolites of Pueraria lobata in rats on peripheral nerve regeneration: in vitro and in vivo studies. J Biomed Mater Res B Appl Biomater. 2008 Jan;84(1):256-62.
68. Klees RF, Salasznyk RM, Ward DF, Crone DE, Williams WA, Harris MP, et al. Dissection of the osteogenic effects of laminin-332 utilizing specific LG domains: LG3 induces osteogenic differentiation, but not mineralization. Exp Cell Res. 2008 Feb 15;314(4):763-73.

Figure 1.

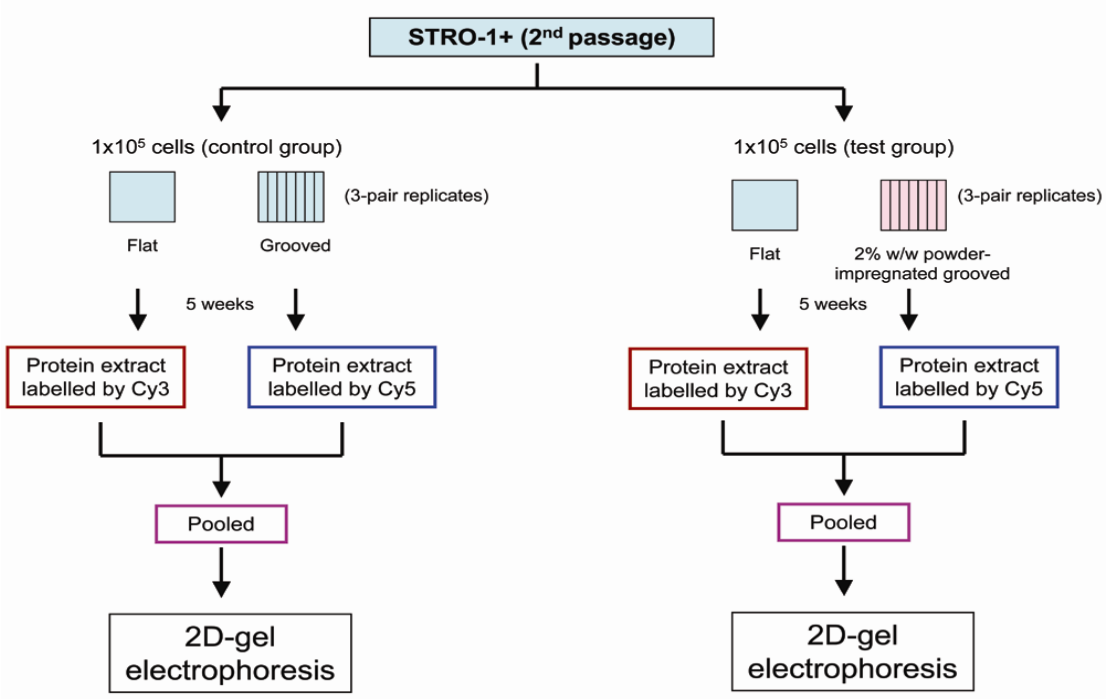

Figure 2.

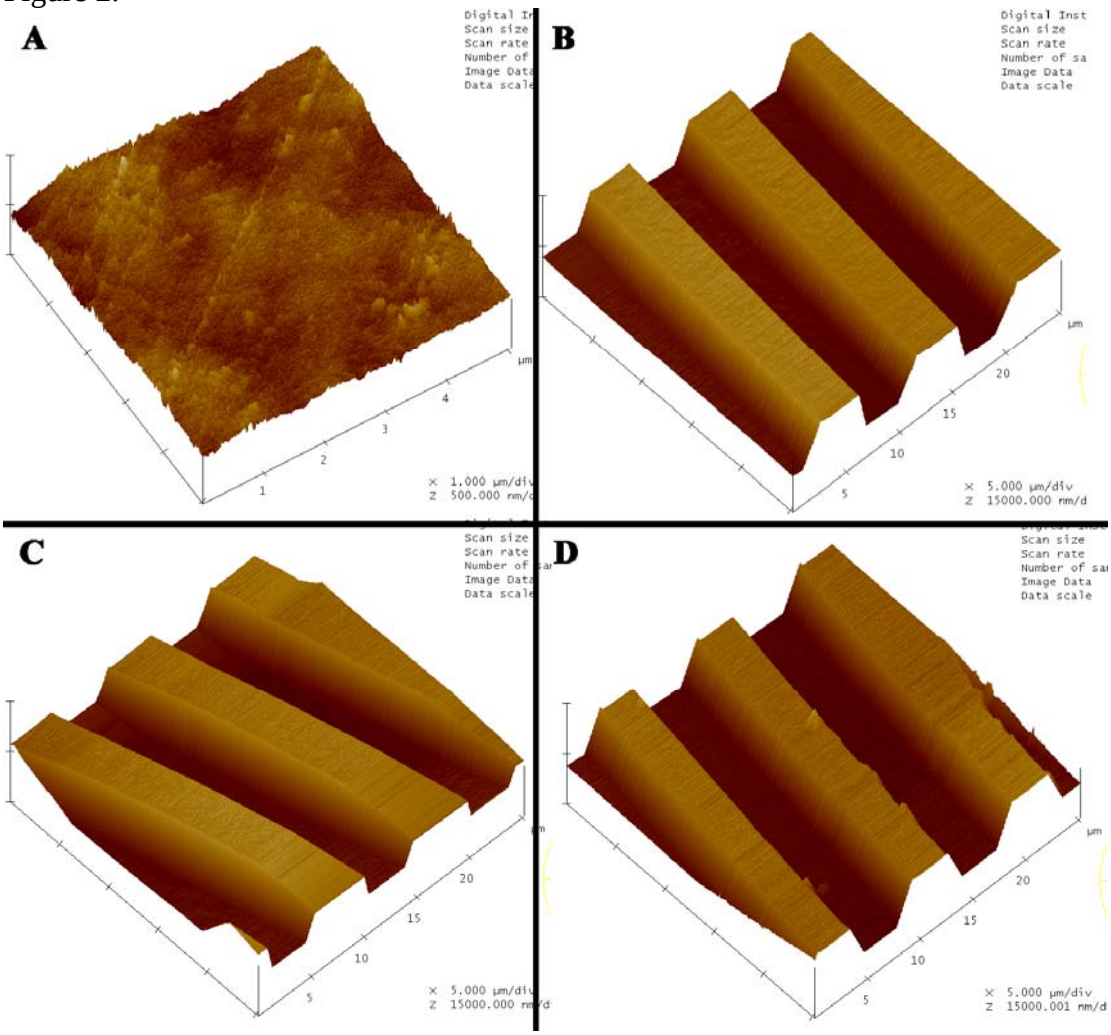

Figure 3.

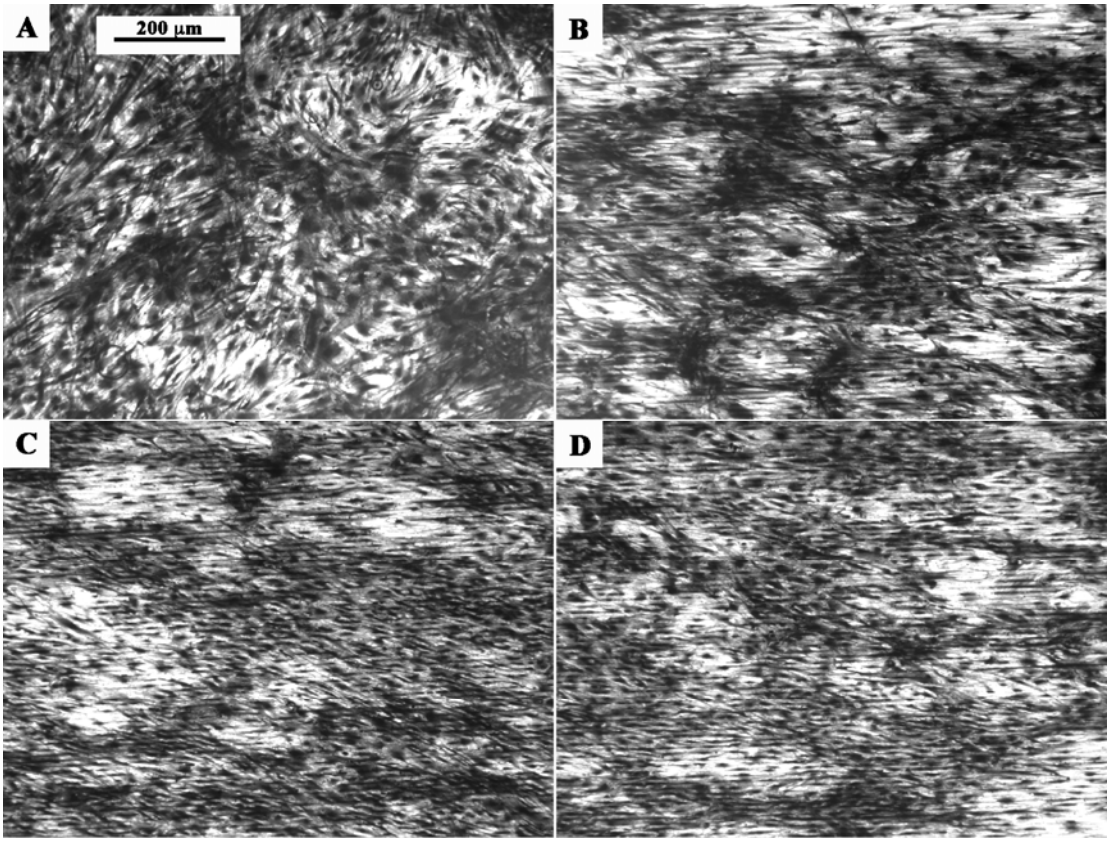

Figure 4.

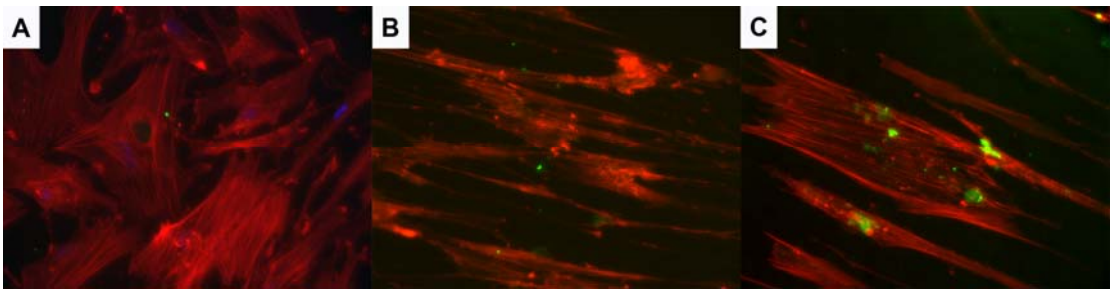

Figure 5.

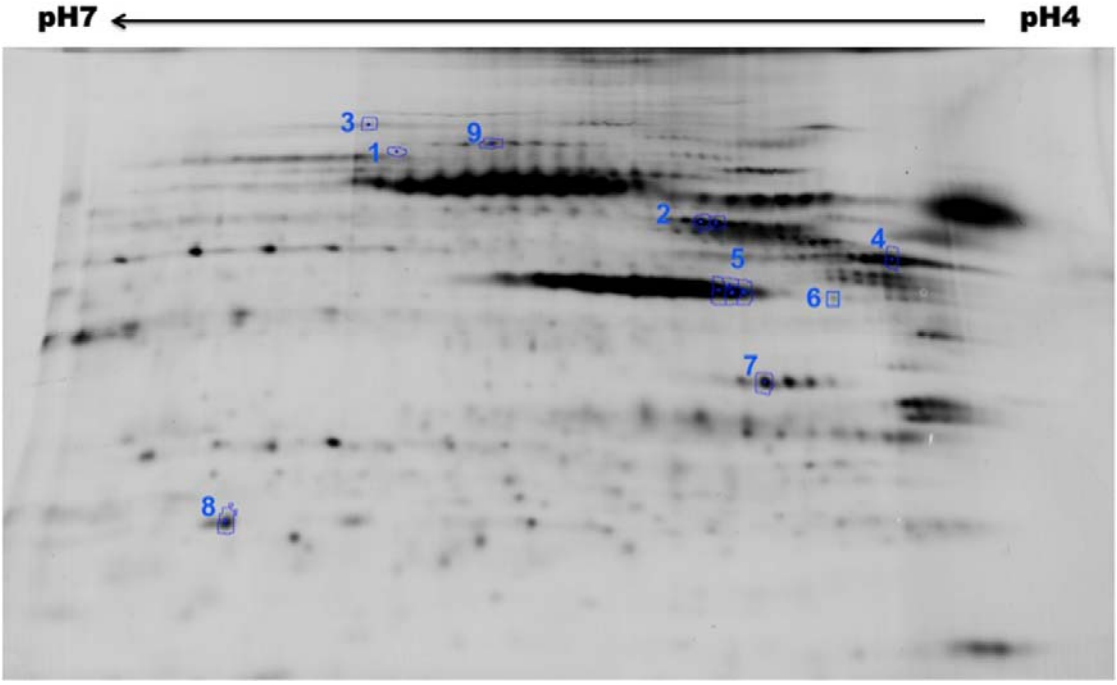

Figure 6.

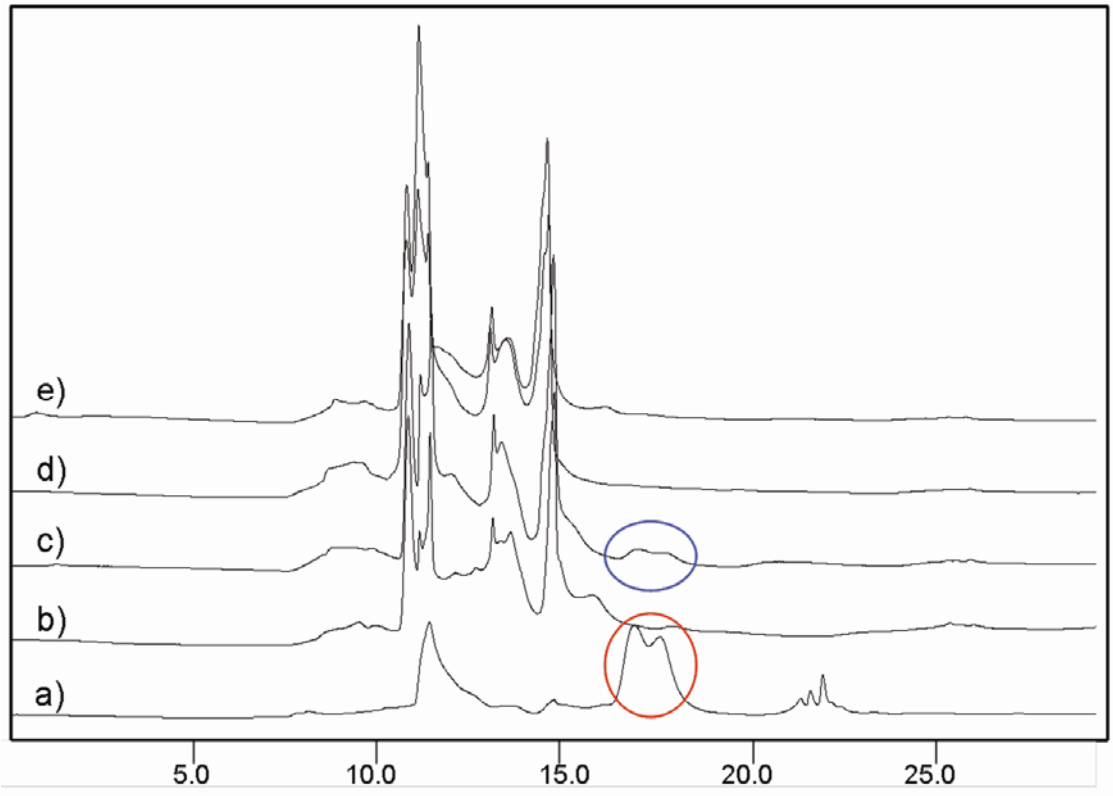

Figure 7.

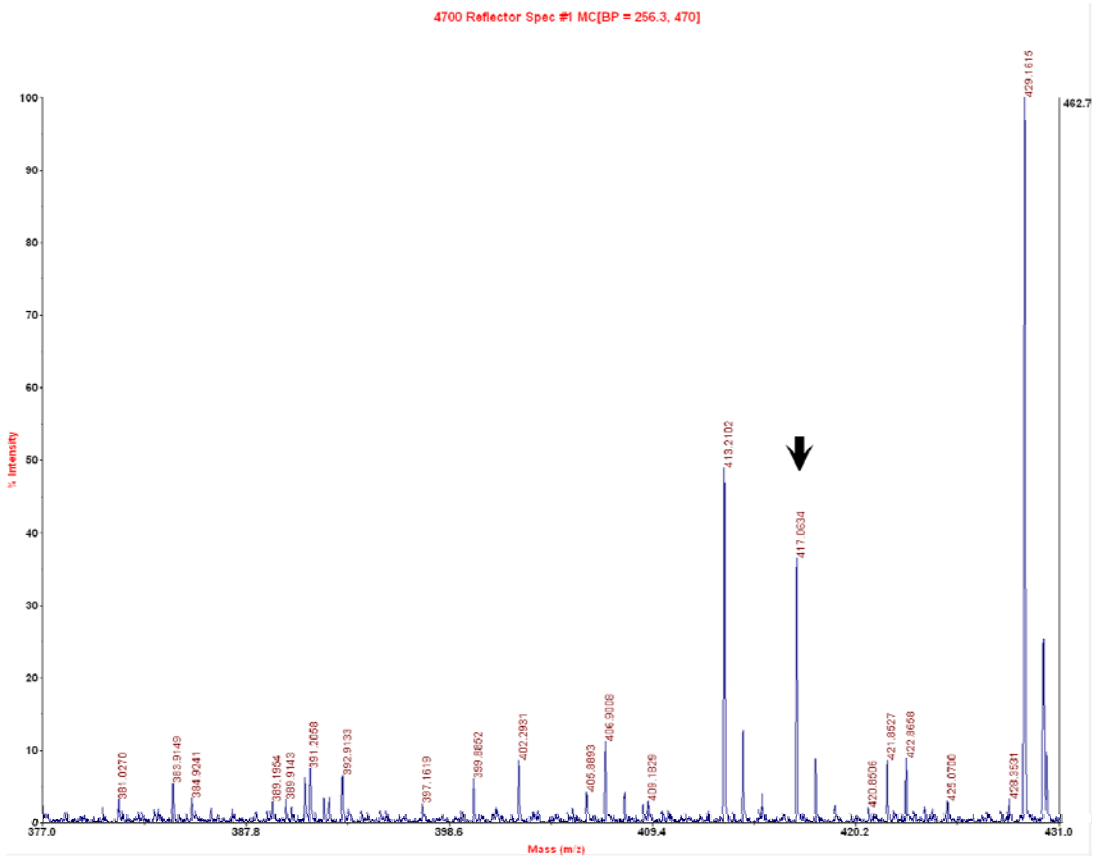
4700 Reflector Spec #1 MC[BP = 256.3, 470]
% Intensity
Mass (m/z)
429.1615
462.7
419.2102
417.0634
381.0270
383.9149
384.9041
389.1954
389.9143
391.2658
392.9133
397.1619
399.8652
402.2931
405.8893
406.9008
409.1829
420.8506
421.8527
422.9658
425.0700
428.3531
377.0
387.8
398.6
409.4
420.2
431.0
100
90
80
70
60
50
40
30
20
10
0

No.	Proteins	AV ratio	p-value
1	Gelsolin	-1.55	0.17*
2	Tubulin	-7.63	0.0024
3	Vinculin	3.02	0.018
4	Vimentin	12.46	0.0025
5	Actin	2.02	0.48*
6	Laminin binding protein	4.59	0.020
7	Annexin V	1.89	0.28*
8	Cofilin	5.39	0.015
9	Myosin head domain containing protein	-1.55	0.042

Table 1.